Electronic Supplementary Material (ESI) for Journal of Materials Chemistry C.

Supporting Information

High efficient green electroluminescence of iridium(III) complexes based on (1*H*-pyrazol-5-yl)pyridine derivatives ancillary ligands with low efficiency roll-off

Ning Su[1], Guang-Zhao Lu[1], You-Xuan Zheng[1,2]*

[1]*State Key Laboratory of Coordination Chemistry, Collaborative Innovation Center of Advanced Microstructures, School of Chemistry and Chemical Engineering, Nanjing University, Nanjing 210023, People's Republic of China*

[2]*Shenzhen Research Institute of Nanjing University, Shenzhen 518057, P. R. China*

**E-mail: yxzheng@nju.edu.cn*

Contents

Experimental details

General Information All solvents were carefully dried and distilled prior to use. Commercially available reagents were used without further purification unless otherwise stated. All reactions were performed under nitrogen atmosphere and were monitored by thin-layer chromatography. ^{1}H NMR spectra were measured on a Bruker AM 400 spectrometer. An electrospray ionization (ESI) mass spectrometer (LCQ fleet, Thermo Fisher Scientific) was used to record mass spectra (MS) for the ligands. High-resolution mass spectra (HRMS) (Agilent 6540 UHD Accurate-Mass Q-TOF LC/MS) were recorded for the complexes. UV-visible absorption and photoluminescence spectra were obtained using a Shimadzu UV-3100 and a Hitachi F-4600 spectrophotometer, respectively. The phosphorescence quantum yields were determined in nitrogen degassed CH_2Cl_2 at 298 K against *fac*-Ir(ppy)$_3$ as a reference (Φ_P = 0.40). The decay lifetimes were determined on an Edinburgh Instruments FLS-920 fluorescence spectrometer in degassed CH_2Cl_2 at room temperature with time-corrected single-photon-counting (TCSPC) measurement. The thermogravimetric analysis (TGA) was performed with a NETZSCH STA449 apparatus from 25 to 800 ^{o}C at a heating rate of 10 ^{o}C/min under nitrogen atmosphere. A conventional three-electrode configuration, consisting of a polished platinum carbon electrode as working electrode, a Pt wire counter electrode, and a reference electrode of $Ag/AgNO_3$ (0.1 M), were used to record cyclic voltammetry data in nitrogen-deaerated CH_3CN solution with 0.1 M $[Bu_4N]ClO_4$ as the supporting electrolyte and ferrocene as internal standard at a scan rate of 50 mV/s. The HOMO and LUMO energy levels were calculated using the equation E_{HOMO} (eV) = -(E_{ox} + 4.8) eV and E_{LUMO}(eV) = E_{HOMO} + E_g^{opt}.

X-ray Crystallography. The crystallographic data were collected on a Siemens SMART CCD diffractometer (Bruker Daltonic Inc.) at room temperature using graphite-monochromated Mo Kα radiation (λ= 0.710 73 Å). The cell parameters were retrieved using SMART software and refined using SAINT on all observed reflections. Absorption corrections were performed with SADABS supplied by Bruker. All the calculations for the structure determination were carried out using the SHELXTL package. Initial atomic positions were located by Patterson method using XS program, and the structures of the complexes were refined anisotropically by the leastsquares method. Hydrogen atoms were fixed in calculated positions and refined as riding atoms with uniform U_{iso} values.

Theoretical Calculation. The density functional theory (DFT) and time-dependent DFT (TD-DFT) calculations were carried out with Gaussian 09 software package. The geometries of the ground state (S_0) were fully optimized with the B3LYP exchange-correlation functional using the LANL2DZ basis set for iridium atom and the 6-31G** basis set for the other atoms both in vacuum and in CH_2Cl_2 (C-PCM27 solvent model). Vibrational frequency calculations were performed to validate that they are minima on potential energy surface. On the basis of the optimized S_0 molecular structures in solvent, TD-DFT calculation was performed. Solvent effect was also considered by using C-PCM model. Frontier molecular orbitals were visualized using Gauss View, and their quantified compositions in percentage on different parts were given by QMForge.

Fabrication of the OLEDs Device Indium tin oxide (ITO) coated glass with a sheet resistance of 15 Ω sq^{-1} was used as the anode substrate. Successively, HATCN (hexaazatriphenylenehexacabonitrile) (5 nm), TAPC (bis[4-(N,N-ditolylamino)-phenyl] cyclohexane, 50 nm), phosphorescent iridium complexes(8 wt%) doped in (4,4',4''-tri(9-carbazoyl) triphenylamine (TCTA) host (20 nm), 1,3,5-tri[(3-pyridyl)-phen-3-yl] benzene (TmPyPB, 40 nm), LiF (1 nm) and Al (100 nm) were evaporated on the substrate, respectively. Current density-voltage-luminance (*J-V-L*) characteristics were measured by using a programmable Keithley source measurement unit (Keithley 2400 and Keithley 2000) with a silicon photodiode.

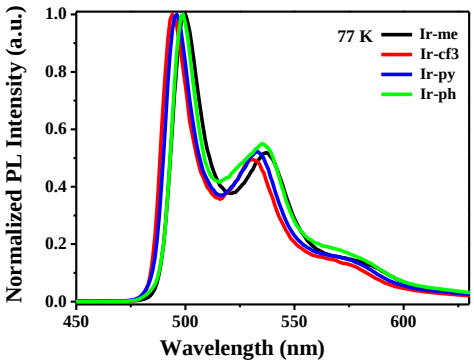

Fig S1. Normalized emission spectra of Ir(III) complexes in dilute DCM (10^{-5} M) at 77 K.

(a)

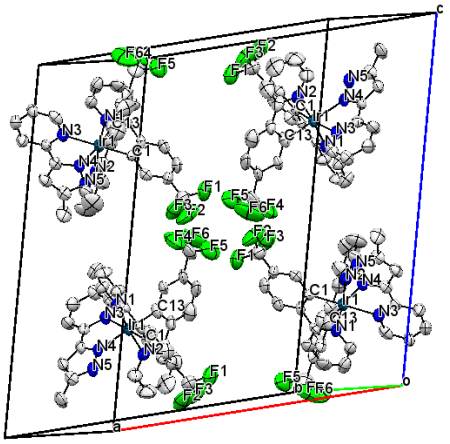

(b)

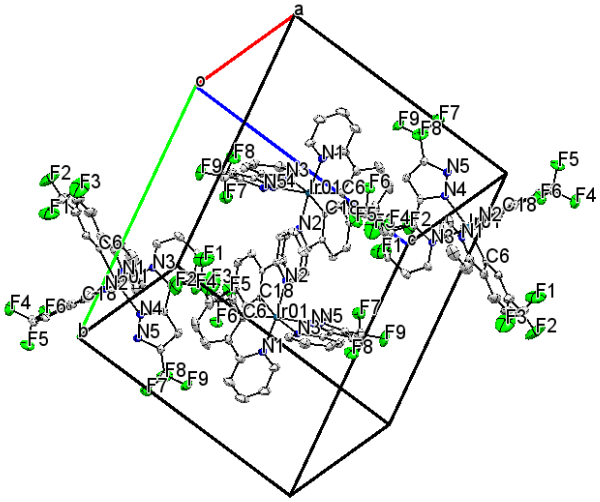

Fig S2. Single crystal packing of **Ir-me** (a) and **Ir-cf3** (b).

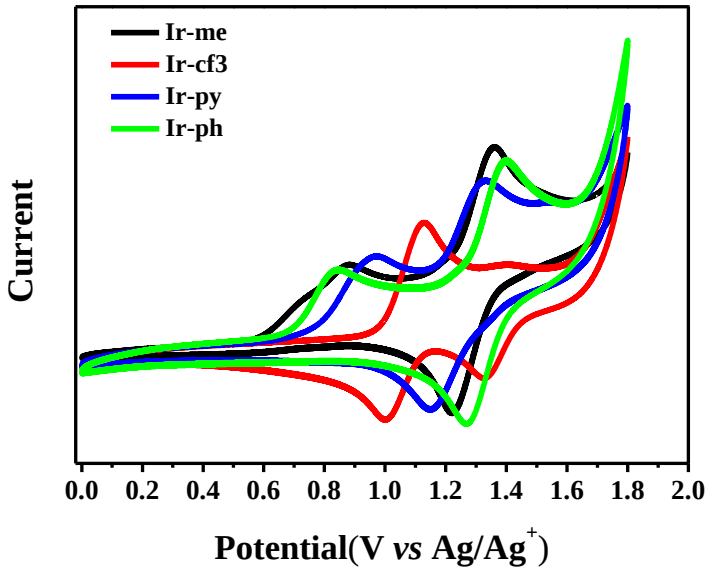

Fig S3. CV curves of Ir(III) complexes.

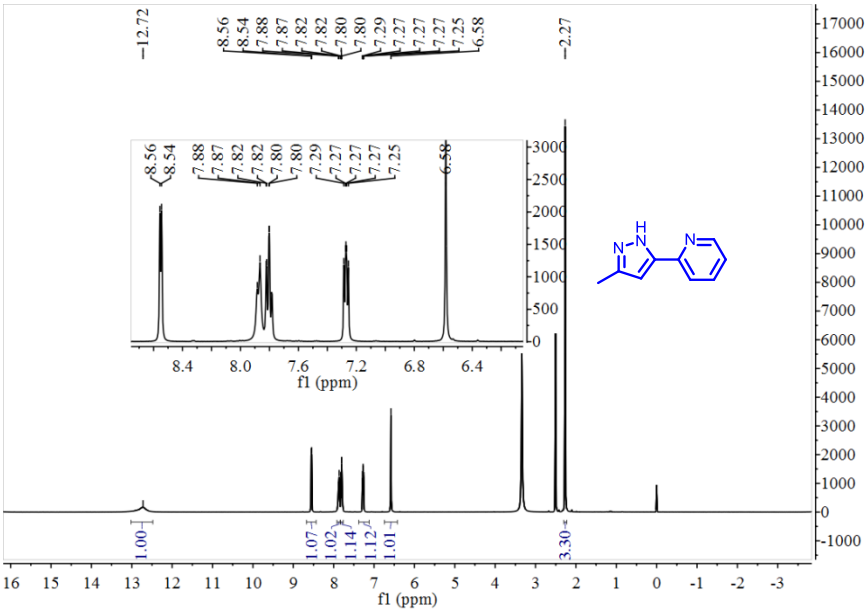

Fig S4. ^{1}H NMR spectrum of mepzpy.

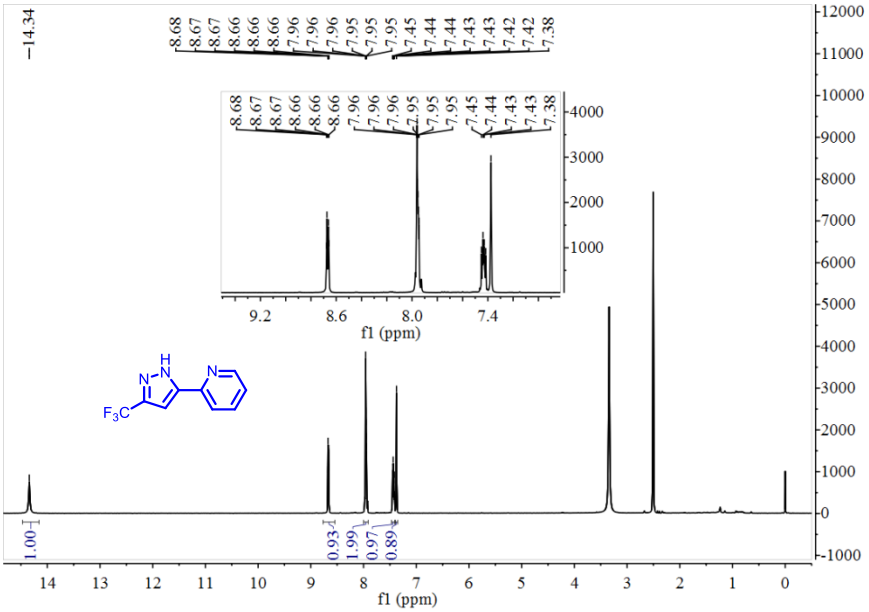

Fig S5. ^{1}H NMR spectrum of cf3pzpy.

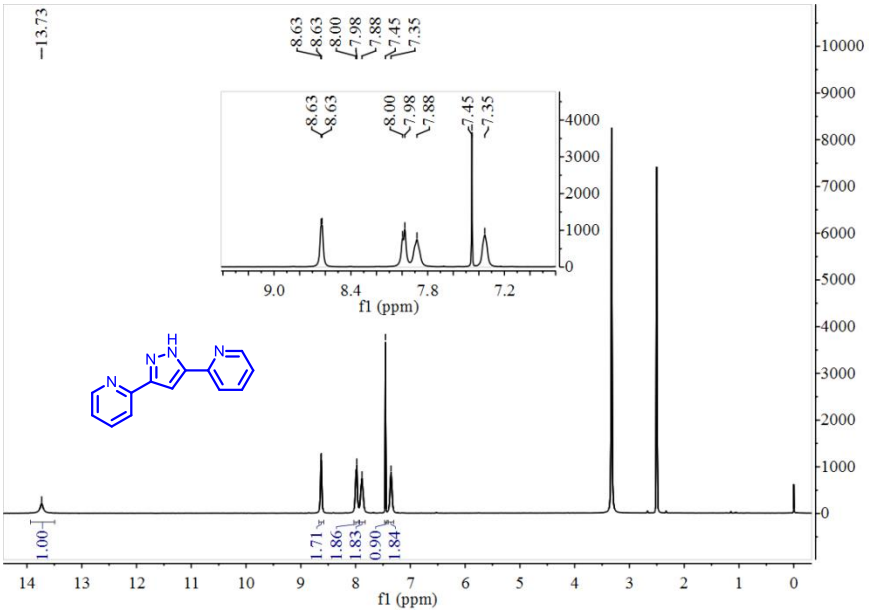

Fig S6. ^{1}H NMR spectrum of pypzpy.

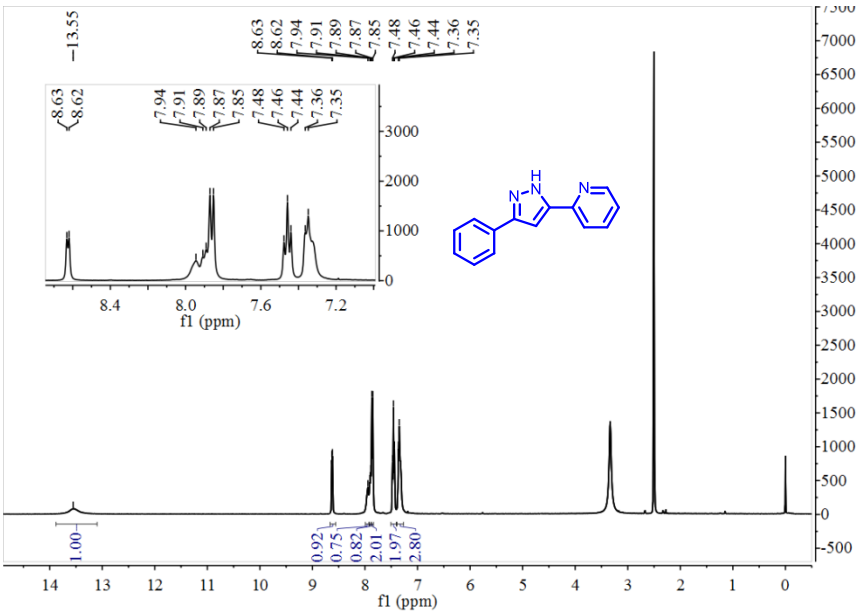

Fig S7. ^{1}H NMR spectrum of phpzpy.

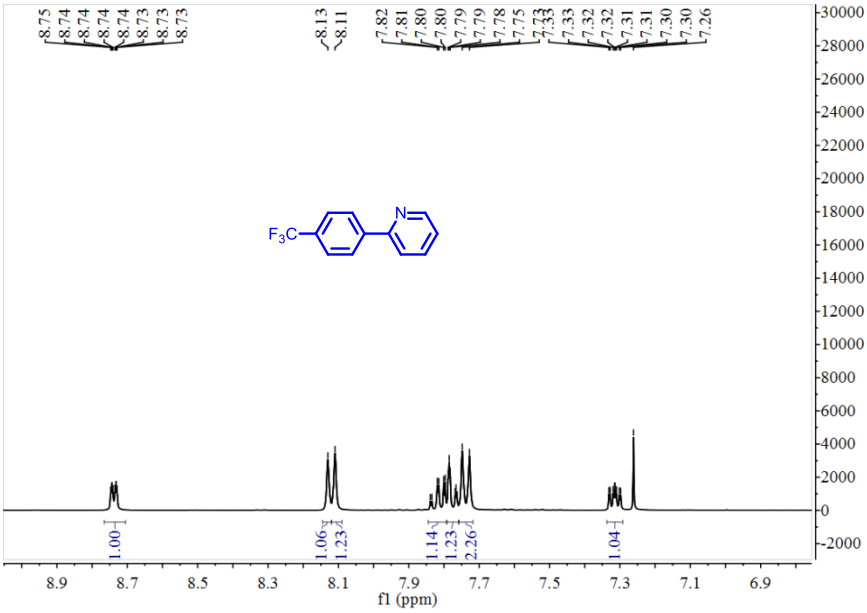

Fig S8. ^{1}H NMR spectrum of tfmppy.

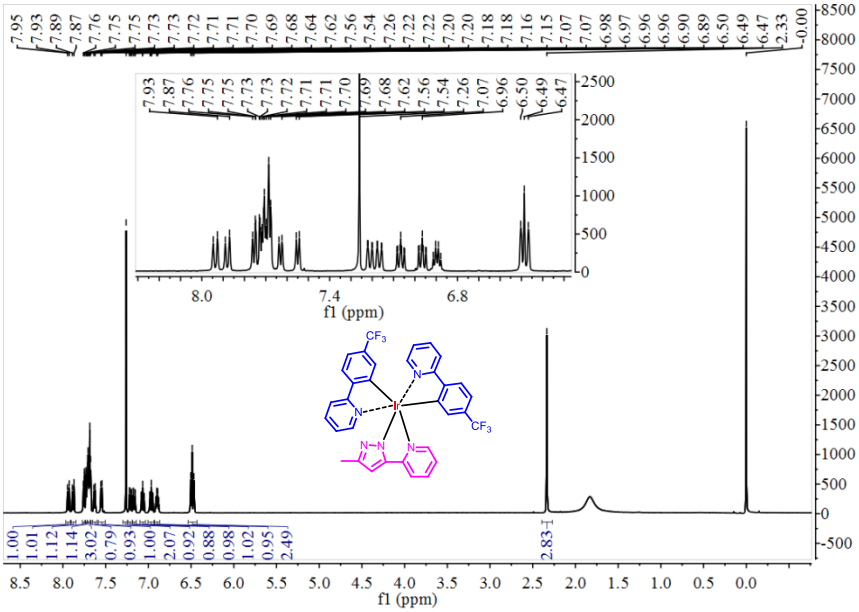

Fig S9. ^{1}H NMR spectrum of **Ir-me**.

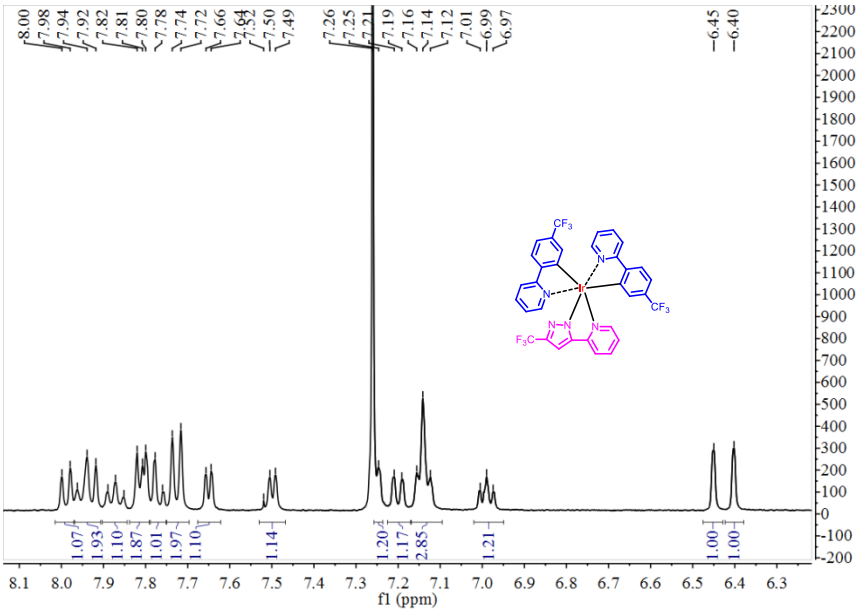

Fig S10. ^{1}H NMR spectrum of **Ir-cf3**.

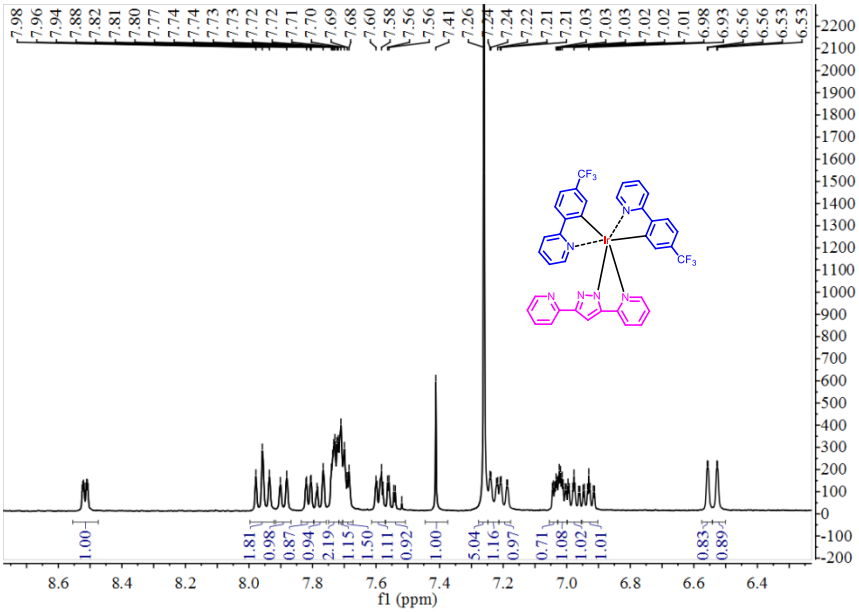

Fig S11. ^{1}H NMR spectrum of **Ir-py**.

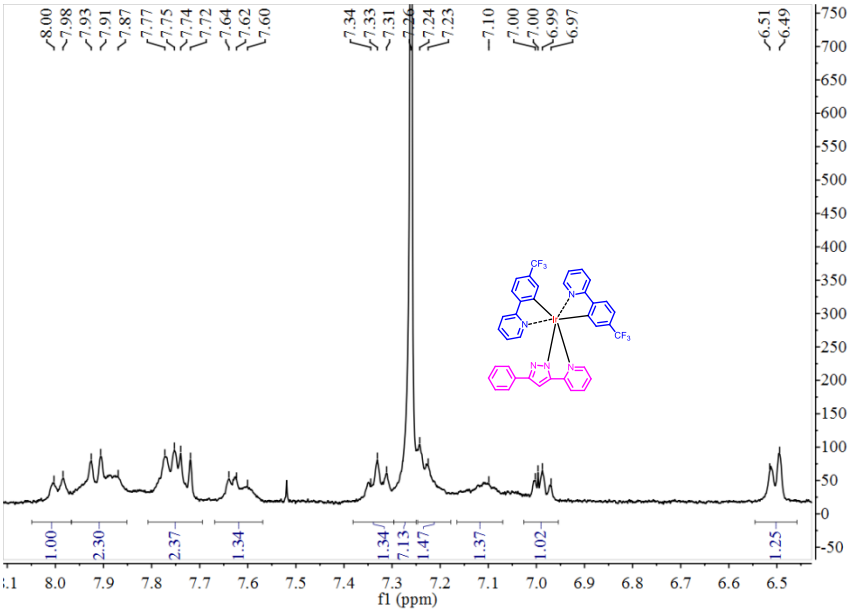

Fig S12. ^{1}H NMR spectrum of **Ir-ph**.

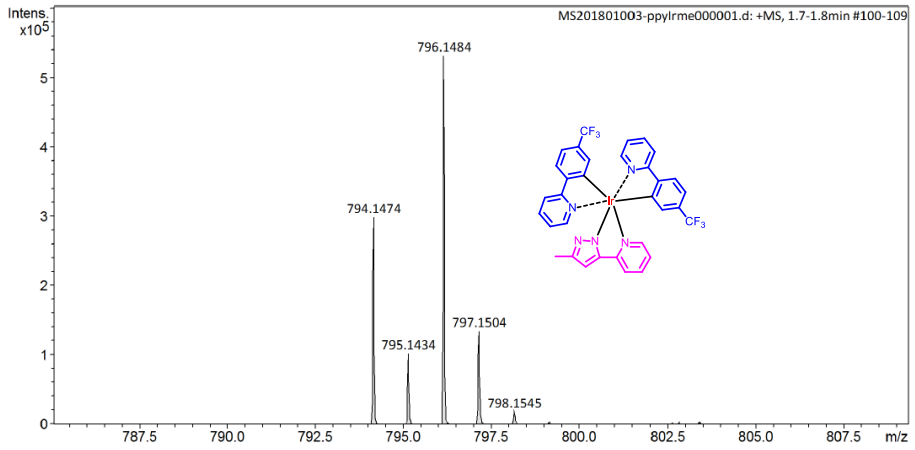

Fig S13. HRMS spectrum of **Ir-me**.

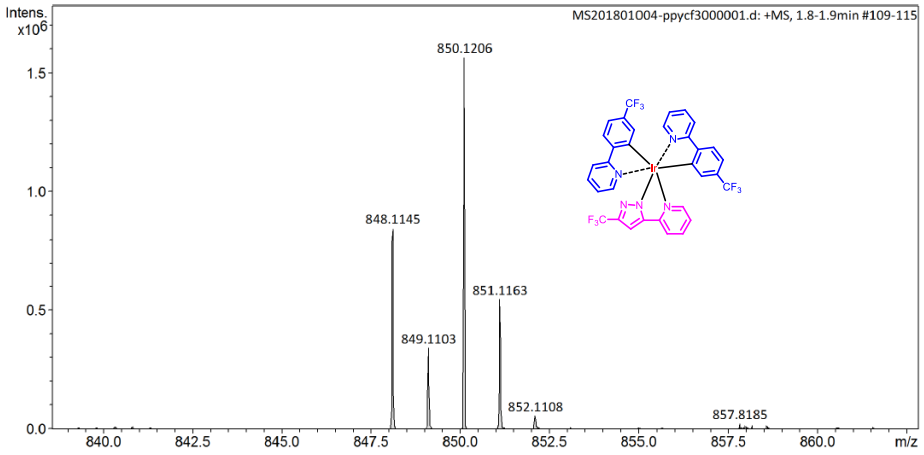

Fig S14. HRMS spectrum of **Ir-cf3**.

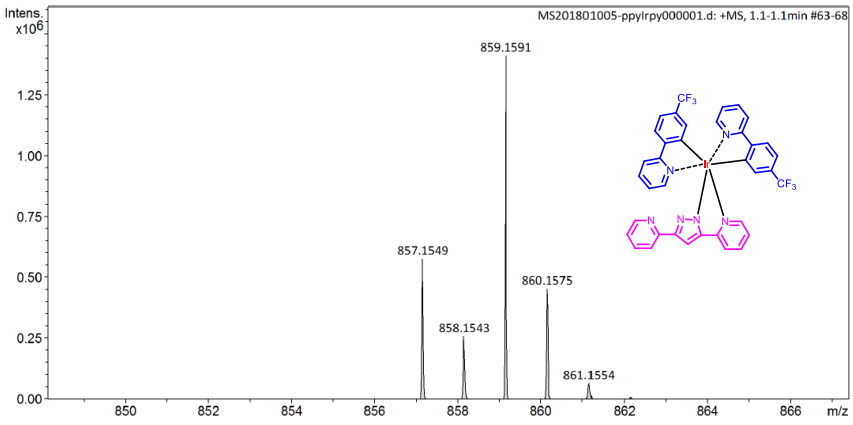

Fig S15. HRMS spectrum of **Ir-py**.

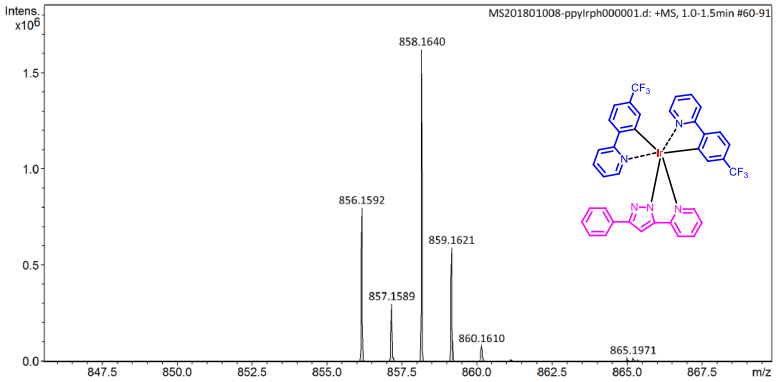

Fig S16. HRMS spectrum of **Ir-ph**.

Table S1. Selected bond length of **Ir-me** complex.

C1-Ir1	2.034 (13)	Ir1—N1	2.043 (10)
C13-Ir1	2.035 (13)	Ir1—N2	2.052 (12)
C1-Ir1-N3	171.2 (5)	Ir1—N3	2.144 (11)
N1-Ir1-N2	174.1 (4)	Ir1—N4	2.103 (9)
C13-Ir1-N4	167.4 (5)		

Table S2. Selected bond length of **Ir-cf3** complex.

C6—Ir01	2.020 (4)	Ir01—N1	2.043 (4)
C18—Ir01	2.023 (4)	Ir01—N2	2.045 (3)
C6—Ir01—N4	170.05 (15)	Ir01—N4	2.102 (3)
N1—Ir01—N2	173.49 (13)	Ir01—N3	2.148 (3)
C18—Ir01—N3	170.94 (15)		

Table S3. Electrochemical data of Ir(III) complexes.

Complexes	E_{ox} (V)[a]	E_g^{opt} (eV)[b]	E_{HOMO} (eV)[c]	E_{LUMO} (eV)[d]
Ir-me	0.90	2.48	-5.55	-3.07
Ir-cf3	1.13	2.48	-5.78	-3.30
Ir-py	0.97	2.48	-5.62	-3.14
Ir-ph	0.85	2.48	-5.50	-3.02

[a]The potential of Fc/Fc^+ *vs* Ag/Ag^+ electrode was measured to be 0.15 V. [b]Calculated from the

absorption band edge of the solution, E_g^{opt} = 1240/$\lambda_{edge.}$ [c]Calculated from empirical equation: E_{HOMO} = -(E_{ox}+ 4.8)eV. [d]Calculated from E_{LUMO} = E_g^{opt} + $E_{HOMO.}$

Table S4. HOMO and LUMO electron cloud density distribution of each fragment of Ir(III) complexes.

Complexes	Orbit	Composition(%)		
		tfmppy	Ir atom	auxiliary ligands
Ir-me	HOMO	16.81	37.65	45.54
	LUMO	94.28	3.42	2.30
Ir-cf3	HOMO	45.70	50.57	3.73
	LUMO	93.96	3.45	2.59
Ir-py	HOMO	11.58	28.69	59.73
	LUMO	94.04	3.49	2.47
Ir-ph	HOMO	5.30	18.26	76.45
	LUMO	94.17	3.46	2.37